Reprinted from

MATERIALS SCIENCE & ENGINEERING A

Materials Science and Engineering A201 (1995) 229–241

An evaluation of the properties of Cr_3Si alloyed with Mo

S.V. Raj

NASA Lewis Research Center, MS 49-1, Cleveland, OH 44135, USA

Received 26 July 1994; in revised form 29 November 1994

ELSEVIER

MATERIALS SCIENCE AND ENGINEERING A

The journal provides an international medium for the publication of theoretical and experimental studies and reviews of the properties and behavior of a wide range of materials, related both to their structure and to their engineering application. The varied topics comprising materials science and engineering are viewed as appropriate for publication: these include, but are not limited to, the properties and structure of crystalline and non-crystalline metals and ceramics, polymers and composite materials.

Types of contributions
Original research work not already published; plenary lectures and/or individual papers given at conferences; reviews of specialized topics within the scope of the journal; engineering studies; letters to the editor.

Subscriptions
Volumes 189–204, each volume containing 2 issues, are scheduled for publication. Prices are available from the publishers upon request. Subscriptions are accepted on a pre-paid basis only. Issues are sent by SAL (Surface Air Lifted) mail wherever this service is available. Airmail rates are available upon request. Please address all requests regarding orders and subscription queries to

ELSEVIER SCIENCE SA

P.O. Box 564, 1001 Lausanne, Switzerland
Telephone: (21) 3 20 73 81
Telex: 450620 ELSA CH Telefax: (21) 3 235 444

Issues are sent by surface mail after air delivery to Argentina, Australia, Brazil, Canada, China, Hong Kong, India, Israel, Japan, Malaysia, Mexico, New Zealand, Pakistan, Singapore, South Africa, South Korea, Taiwan, Thailand and the USA. Airmail rates for other countries are available on request.
For advertising rates apply to the publishers. A specimen copy will be sent on request.

US and Canadian customers may obtain information from the following.

ELSEVIER SCIENCE INC.
Attn.: Journal Information Center, 655 Avenue of the Americas
New York, NY 10010, USA.
Telephone: (212) 633 3750 Telex: 420 643 AEP UI
Telefax: (212) 633 3764.

Abstracting and/or Indexing Services
American Ceramic Society; Cambridge Scientific Abstracts; Chemical Abstracts; Current Contents; Engineering Index; FIZ Karlsruhe; Fluid Abstracts; Fluidex; Glass Technology Abstracts; Inspec/Physics Abstracts; Metals Abstracts; Pascal (Centre National de la Recherche Scientifique); Physikalische Berichte; Research Alert™; Science Citation Index.

ELSEVIER

Materials Science and Engineering A201 (1995) 229–241

MATERIALS SCIENCE & ENGINEERING A

An evaluation of the properties of Cr_3Si alloyed with Mo

S.V. Raj

NASA Lewis Research Center, MS 49-1, Cleveland, OH 44135, USA

Received 26 July 1994; in revised form 29 November 1994

Abstract

The properties of a Cr_3Si alloy designed for the high temperature, high velocity gas flow conditions typical of the operating environment within an aircraft engine are discussed. The alloy composition was obtained by macroalloying Cr_3Si with Mo to improve its high temperature oxidation resistance. Detailed cyclic, isothermal and low temperature "pest" oxidation studies conducted between 773 and 1673 K revealed that the alloy has excellent oxidation properties due to the formation of dual protective oxides scales of Cr_2O_3 at low temperatures and SiO_2 at high temperatures. Preliminary burner rig tests conducted at 1473 K in a 0.3 mach combustion flame indicated that the alloy life is expected to exceed 100 cycles. The alloy exhibits a compressive brittle-to-ductile transition temperature of about 1500 K. The compression strengths vary between 650 MPa at 1500 K and 50 MPa at 1700 K. Preliminary results suggest that the compressive creep strength of the as-cast alloy is equal to or better than $MoSi_2$-reinforced with either SiC_p or SiC_w, while that of the powder metallurgically-processed alloy is comparable only to the unreinforced $MoSi_2$. The room temperature fracture toughness of the alloy was determined to be between 2.0 and 3.0 MPa $m^{1/2}$.

Keywords: Cr_3Si alloy; Creep; Oxidation properties

1. Introduction

The expected advent of high speed civil transport (HSCT) and advanced subsonic aircraft in the 21st century has focussed interest in developing intermetallic alloys with absolute melting points, T_m, in excess of 1875 K. The engines for these aircraft will operate at higher stresses and temperatures in an oxidizing environment for longer periods of time than those in use today. Materials selected for HSCT applications will be chosen because they possess the best balance of properties. These properties include adequate oxidation resistance, a high melting point, low density, ρ, excellent creep resistance, and good ductility and fracture toughness, K_q, at all temperatures. Since inherent oxidation resistance is an important property, a comparison of the parabolic rate constants, k_p, for several oxides shows that materials which form a stable alumina or silica scale are the most likely to possess good oxidation resistance due to their low values of k_p (Fig. 1) [1]. As a result, aluminides and silicides are generally believed to hold the best promise among the various categories of intermetallics in developing suitable materials for the desired HSCT applications.

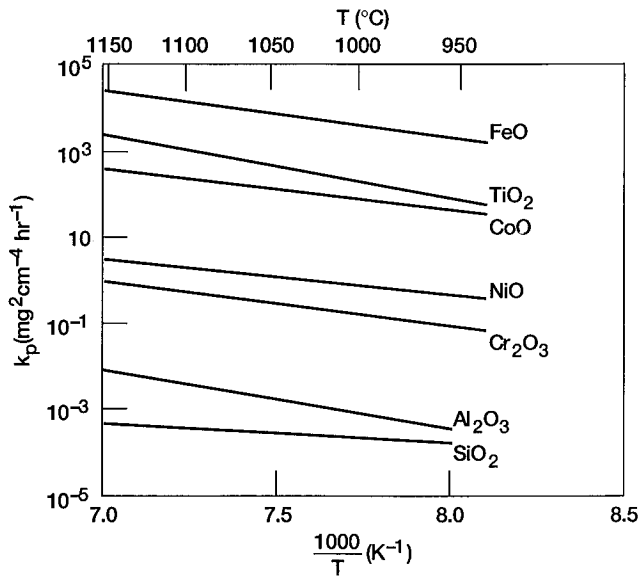

Fig. 1. Arrhenius plot showing typical parabolic rate constants for several oxides [1].

Elsevier Science S.A.
SSDI 0921-5093(95)09767-8

Table 1
Selection criteria used for choosing the silicide system

Property	Benchmark	Remarks
Melting point	$T_m \geq 1973$ K	
Density	$\rho \leq 8.0$ Mg m^{-3}	Equal to or less than superalloys
Crystal structure	cubic	Provides isotropic thermal expansion properties
Phase diagram	Solid solubility	Provides alloying capability
Thermal conductivity	$\beta \geq 8$ W m^{-1} K^{-1}	Equal or better than superalloys
Oxidation resistance	(a) Should not disintegrate catastrophically or "pest"	
	(b) Should form a protective oxide scale	
Creep strength to ensure less than 1% creep in 100 h	$\sigma \geq 100$ MPa[a]	Equal or better than superalloys

[a]Based on creep data for PWA 1480 at 1373 K [4].

The objective of the present study was to identify a silicide system for its potential as an aircraft engine material. Preliminary results on the development and properties of a chromium silicide alloy were discussed in an earlier paper [2,3] and additional data are presented here.

1.1. System selection

Table 1 lists the broad selection criteria used in choosing the alloy system. These design values were chosen to ensure that the alloy had properties comparable to or better than a Ni–base superalloy. In particular, the desired creep strength, σ, of 100 MPa is based on that reported for PWA 1480 at 1373 K [4]. Several stable silicides possess $T_m \geq 1973$ K (Table 2). Among these, Cr_3Si was found to satisfy most of the criteria listed in Table 1. It has a cubic A15 crystal structure, $\rho \approx 6.5$ Mg m^{-2} [5], $T_m \approx 2043$ K and a solid solubility limit of about 3 at.% (Fig. 2) [6]. Some early work suggested that Cr_3Si had good oxidation resistance [7] although the data were insufficient to make any reasonable conclusion on the oxidation properties of the material. At the time this study commenced, there were few or no mechanical property data on Cr_3Si reported in the literature. In contrast, most of the other silicides did not satisfy many of the requirements given in Table 1. Although V_3Si satisfied most of the selection criteria listed in Table 1, it was not selected primarily because it is unlikely that this material would have good oxidation resistance at high temperatures as a result of the formation of a non-protective low melting point V_2O_5 scale during oxidation. Among the other potential silicide systems, $MoSi_2$ has received considerable attention in recent years primarily because of its excellent high temperature oxidation resistance above 973 K [8]. Despite its excellent high temperature oxidation resistance, it does not satisfy many of the criteria listed in Table 1. For example, the alloy undergoes catastrophic disintegration or "pest" between 673 and 873 K [9,10]. In addition, it is a line compound and possesses a tetragonal $C11_b$ crystal structure (Table 2).

A few preliminary studies were conducted on Mo_5Si_3, RuSi, Ti_5Si_3 and Y_5Si_3 despite the fact that they do not

Table 2
Silicide systems with $T_m > 1973$ K

System	Phase diagram	Phase	Structure	T_m (K)	ρ (Mg m^{-3})
B-Si	Line	SiB_6	SiB_6	2123	2.3
	Solid soln.	SiB_n	B	2293	–
C-Si	Line	SiC	B3	2818	3.2
Cr-Si	Solid soln.	Cr_3Si	A15	2043	6.5
Hf-Si	Line	Hf_2Si	C16	2356	–
	Line	Hf_3Si_2	$D5_d$	2573	–
	Line	Hf_5Si_4	Zr_5Si_4	2593	–
	Line	HfSi	B27	2415	–
Mo-Si	Line	Mo_3Si	A15	2293	8.4
	Solid soln.	Mo_5Si_3	D8m	2453	8.2
	Line	α-$MoSi_2$	$C11_b$	2293	6.3
Nb-Si	Solid soln.	β-Nb_5Si_3	D8b	2793	7.2
	Solid soln. (?)	α-Nb_5Si_3	$D8_l$	2213	7.2
	Line	$NbSi_2$	C40	2213	5.7
Re-Si	Line	Re_2Si	–	2083	–
	Line	$ReSi_{1.8}$	$C11_b$	2213	10.7
Ru-Si	Line	β-RuSi	B2	2123	8.5
	Line	α-RuSi	B20	1963	8.5
Ta-Si	Line	$TaSi_2$	C40	2313	9.1
	Line	β-Ta_5Si_3	$D8_m$	2823	13.1
	Line	α-Ta_5Si_3	$D8_l$	2433	13.1
	Line	Ta_2Si	C16	2713	13.5
	Line	Ta_3Si	PTi_3	2613	–
Ti-Si	Solid soln.	Ti_5Si_3	$D8_8$	2403	4.4
	Line	Ti_5Si_4	Zr_5Si_4	2193	–
V-Si	Solid soln.	V_3Si	A15	2198	5.7
	Line	V_5Si_3	$D8_m$	2283	5.3
W-Si	Line	WSi_2	$C11_b$	2433	9.9
	Line (?)	W_5Si_3	$D8_m$	2593	–
Y-Si	Solid soln.	Y_5Si_3	$D8_8$	2123	4.5
	Line	Y_5Si_4	Ge_4Sm_5	2113	–
	Line (?)	YSi	B_f	2108	4.5
Zr-Si	Line	β-ZrSi	B_f	2483	5.7
	Line	β-Zr_5Si_4	–	2523	5.4
	Line	Zr_3Si_2	$D5_\alpha$	2488	–
	Line	Zr_2Si	C16	2198	6.0

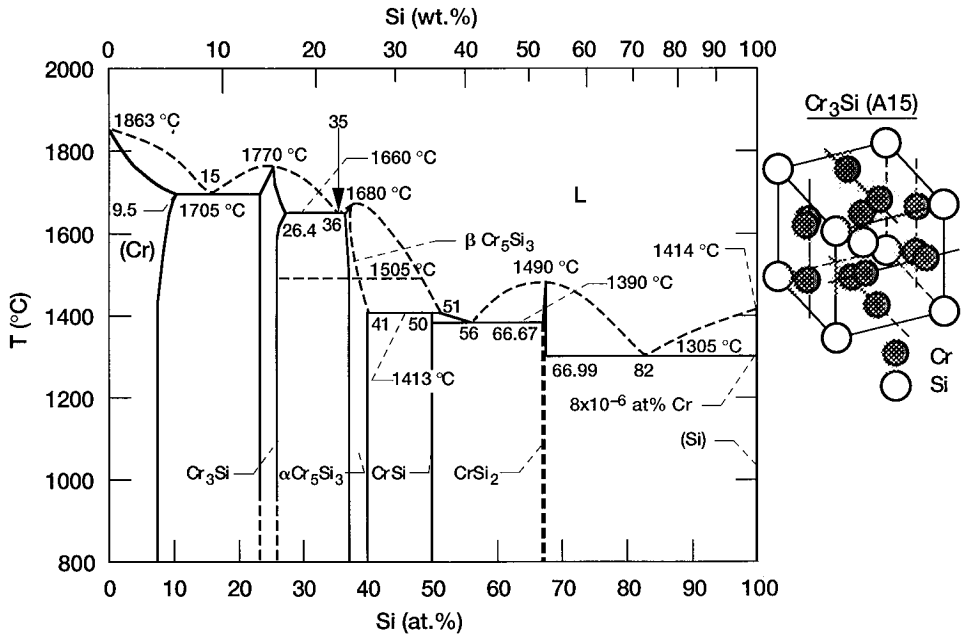

Fig. 2. Chromium–silicon phase diagram [6] and the A15 crystal structure of Cr_3Si.

satisfy some of the criteria listed in Table 1. These materials were chosen in part because their higher melting temperatures although other factors such as solid solution region (Mo_5Si_3, Ti_5Si_3 and Y_5Si_3), B2 crystal structure (RuSi) and potential for good oxidation resistance (Ti_5Si_3 and Y_5Si_3) were also considered (Table 2). The early results from these studies suggested that Mo_5Si_3, Ti_5Si_3 and Y_5Si_3 were difficult to process. In addition, it was observed from a few oxidation experiments that RuSi did not develop a protective SiO_2 scale at 1473 K and instead formed RuO_2. An additional factor in the case of RuSi was the high cost of Ru. These studies were discontinued based on the above observations.

1.2. Brief review of existing mechanical properties and oxidation data on Cr_3Si and its alloys

Several reports have been published since 1988 which suggest that the Cr_3Si alloy system is beginning to draw the attention of a number of research groups [11–21]. However, relative to $MoSi_2$, even this information is sparse. Fleisher and Zabala [11] obtained a value of 350 GPa for the room temperature Young's modulus, E, of Cr_3Si. They also reported that the microhardness of Cr_3Si falls from 1200 HV at room temperature to 200 HV at 1373 K. From a study of the compression properties of single and polycrystalline Cr_3Si, Chang and Pope [12] concluded that the material was brittle below 1473 K but exhibited compression strengths varying between 175 and 450 MPa in the temperature range 1523 to 1673 K. They also observed that deformation occurs on the {001} slip planes along the ⟨010⟩ crystallographic directions. Anton et al. [13–16] reported that the Cr_3Si exhibits a change in the creep stress exponent, n, from $n \approx 3.4$ at 1473 K to $n \approx 2.1$ at 1673 K. The apparent activation energy for creep, Q_A, was reported to be about 500 kJ mol^{-1} [13,14]. Interestingly, judging from the single datum point for a Cr–39(at.%) Mo–23 Si alloy[1] [16], it would appear that Mo significantly improves the creep properties of Cr_3Si [13–16]. Using bend test data, they confirmed the earlier observations by Chang and Pope [12] that Cr_3Si is brittle up to 1473 K [13]. Measurements of the fracture toughness of Cr_3Si and Cr–Cr_3Si two-phase alloys using a Vickers hardness indentation technique showed that $K_q \approx 5.5$–8.0 MPa m$^{1/2}$ for the Cr–Cr_3Si alloys while $K_q \approx 1.8$ MPa m$^{1/2}$ for Cr_3Si [17]. Bewlay et al. [18,19] have used directional solidification techniques to grow Cr–Cr_3Si in-situ eutectic composites. The properties of this material were not reported. Low values of K_q were also reported for Cr_3Si–Al_2O_3 long fiber composites probably due to poor consolidation of the composites [20].

Although it is often suggested in the literature that Cr_3Si possesses good oxidation resistance, it is surprising to note that there is a sparsity of oxidation data on the material. In a review of the properties of a number of silicides, Kieffer and Benesovsky [21] reported that $CrSi_2$ formed a "greenish porous coating" after oxidation at 1473 K for 4 h. From this observation, it was concluded that chromium silicides were not expected to possess good oxidation resistance. A subsequent study reported that Cr_3Si gained 0.5 and 7.3 mg cm^{-2} after a

[1]Unless otherwise stated, all compositions are reported in at.%.

100 h exposure at 1273 and 1533 K, respectively, which suggested that the alloy had acceptable oxidation resistance along with other silicides, such as $MoSi_2$ and $TiSi_2$ [7]. More recent isothermal oxidation data obtained in flowing air suggest that Cr_3Si has good oxidation resistance [22]. Cyclic oxidation data published by Anton and Shah [13] revealed that Cr_3Si and $MoSi_2$ exhibit similar specific weight change, $\Delta W/A$, where ΔW is the weight change due to oxidation and A is the oxidized surface area, with time at 1423 K for at least 50 cycles.

2. Choice of alloy composition

2.1. Preliminary studies

Oxidation resistance at operating temperatures is an important property in aircraft engine applications. In order to determine whether Cr_3Si forms a protective SiO_2 scale at high temperatures, small chunks of as-cast Cr_3Si were oxidized at 1473 and 1773 K for periods ranging between 2 and 4 h in air. The oxide scale was analysed by X-ray diffraction (XRD) to identify the constituents. In all instances, Cr_2O_3 was the primary oxide constituent although a little SiO_2 was detected in a specimen exposed at 1773 K for 4 h. In the latter case, Cr loss was substantial enough to cause the specimen to melt due to a change in composition. These initial studies established that Cr_3Si has poor oxidation resistance above 1473 K since it does not form a protective SiO_2 scale due to the slower rate of formation of SiO_2 compared to Cr_2O_3. It was hypothesized from these observations that the open crystal structure of Cr_2O_3 allows easy oxygen diffusion into the bulk, where more Cr is oxidized at a faster rate than the increasingly Si-rich matrix. It is pertinent to note that the more Si-rich $CrSi_2$ also does not form a protective SiO_2 layer [23]. In this case, it was observed that Cr_2O_3 grew rapidly with the simultaneous evaporation of CrO_2 and CrO_3 and no selective oxidation of the islands of Si were observed below 1473 K. Above 1473 K, although an inner layer of SiO_2 was observed below an outer layer of Cr_2O_3, it did not adhere very well to the substrate. Thus, in view of the poor oxidation resistance of $CrSi_2$ [23], it is not surprising that Cr_3Si also possesses poor oxidation resistance.

Attempts to improve the oxidation resistance of Cr_3Si by replacing the Cr with Al, Ti, and Y resulted in the formation of complex low melting point compounds. However, Mo substitution for Cr by weight appeared to improve the spalling resistance of the oxide scale. Thus, the Cr_3Si alloyed with Mo was studied more extensively.

2.2. Conceptual alloy design

In the intended application as an aircraft engine material, the component is expected to be subjected to high velocity combustion gases. A major objective of the present study is to ensure that the Cr_3Si–base alloy will form two protective oxides, Cr_2O_3 and SiO_2, at low and high temperatures, respectively. Under this alloy design concept, the desired aim was to alloy Cr_3Si so that the low temperature protective Cr_2O_3 oxide will volatilize at high temperatures especially under a high velocity combustion flame to allow the formation of a protective SiO_2 oxide scale. It was assumed that replacing chromium with sufficient amount of molybdenum by weight would increase the volatility of chromium and molybdenum oxides and lead to the formation of a sufficient amount of a silicon-rich layer at the surface. Subsequent oxidation of Si could lead to the formation of a protective SiO_2 scale at high temperatures. At lower temperatures, the formation of a stable protective Cr_2O_3 layer could provide the necessary oxidation resistance.

2.3. Burner rig tests

In order to verify the alloying concept, the alloys were tested in a burner rig since this type of experiment approximates actual operating conditions within an aircraft engine. Several Cr–Mo–Si alloys containing 0 to 33% Mo mainly to replace chromium were prepared either by arc-melting or induction-melting appropriate amounts of chromium, molybdenum and silicon under argon[2]. The melts were cast directly into burner rig specimens varying between 50 and 180 mm long and about 10.5 mm in diameter (Fig. 3). The hot tops were not removed from some of the cast rods due to the brittleness of the alloys (Table 3) .

The burner rig tests were conducted at 1473 K using a mixture of JP5 jet fuel and preheated air maintained at a combustion pressure of 0.007 MPa. Combustion gases exiting the combustor nozzle were allowed to impinge on a single rotating specimen ($\approx$ 200 r.p.m.) at a velocity of mach 0.3 (Fig. 4(a)). The specimens were subjected to 1 h cycles between room temperature and 1473 K, where each cycle consisted of 55 min at the high temperature followed by a 5 min quench to room temperature in forced air. Tests were continued to a maximum of 100 cycles. Table 3 compares the burner rig failure life for several Cr–Mo–Si alloys. It is evident that Alloy 22 containing 30.3% Mo and 30.0% Si

[2]The Cr, Mo and Si used during the course of this investigation were obtained from different stock of material depending on their availability. Typical ranges of purity for the raw materials were determined to be Cr: 99.64–99.99 (wt.%), Mo: 99.67–99.98%, and Si: 99.952–99.9999%.

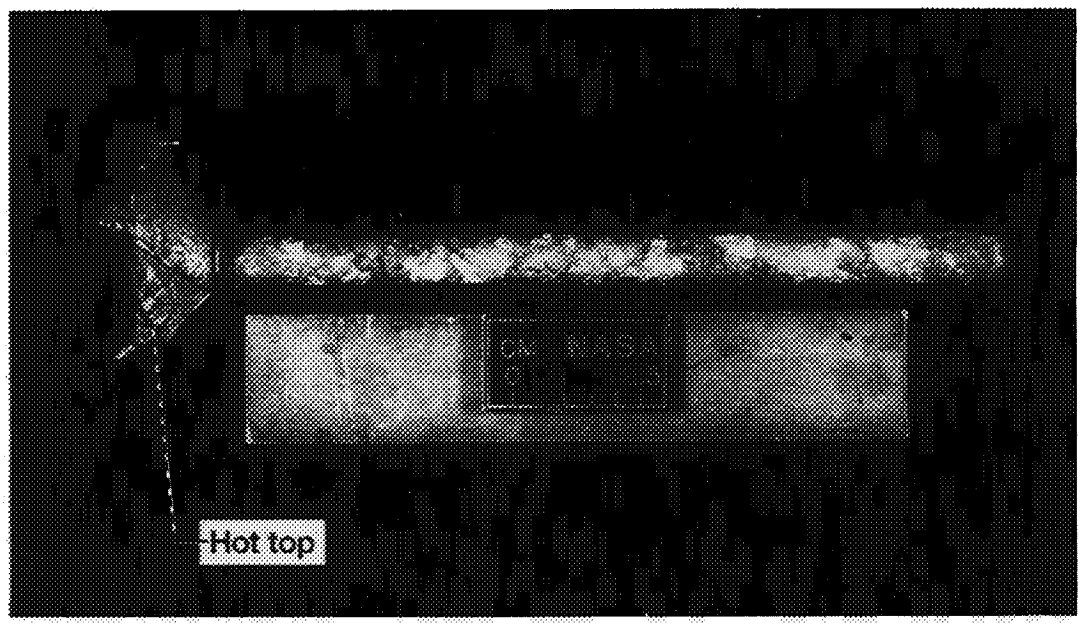

Fig. 3. As-cast and untested $Cr_{17}Mo_{17}Si_{66}$ burner rig specimen. Large grains are visible at the surface.

(to be designated $Cr_{40}Mo_{30}Si_{30}$) lasted 100 cycles without failure despite the fact that the as-cast material had shrinkage cracks. In contrast, Cr_3Si had a burner rig life of less than 4 cycles, while Alloy 23 containing 33.3% Mo and 33.3% Si, corresponding to the center of the Gibbs triangle, lasted 81 cycles. Alloy 24 containing 16.7% Mo and 66.7 Si failed after 20 cycles. X-ray photoelectron spectroscopy (XPS) studies conducted on Alloy 22 after exposure for 20 cycles in a burner rig showed that Cr and Mo were absent in region A of the specimen subjected to the direct impact of the combustion flame (Fig. 4(b)). Instead this area consisted primarily of SiO_2, thereby confirming one of the desired objectives of this alloy development program. It should be noted that Cr and Mo were observed in regions (e.g. B in Fig. 4(c)) away from the direct impact of the burner flame. The XPS analysis also revealed a high carbon composition at the surface due to deposition from incomplete combustion of the fuel. It was concluded from these studies that $Cr_{40}Mo_{30}Si_{30}$ is likely to form a protective SiO_2 scale under actual operating conditions. Hence, this alloy composition was chosen for detailed property evaluation.

Table 3
Burner rig failure lives at 1473 K following 1 h cycles

Alloy No.	Nominal composition (at.%)	Cycle life (h)	Remarks
9	Cr 25 Si	<4	Failed
17	Cr 2.5 Mo 24.4 Si	11	Failed
19	Cr 10.5 Mo 26.0 Si	<1	Failed
21	Cr 23.1 Mo 28.6 Si	<3	Failed
22	Cr 30.3 Mo 30.0 Si	100	Test stopped; hot top[a]
23	Cr 33.3 Mo 33.3 Si	81	Failed; hot top[a]
24	Cr 16.7 Mo 66.7 Si	20	Failed; hot top[a]

[a]Specimens tested with their hot tops intact.

3. Physical metallurgy and microstructures

Induction melting was not employed for making the materials used for characterizing the mechanical and oxidation properties owing to crucible reaction with the molten metal. All characterization studies on the $Cr_{40}Mo_{30}Si_{30}$ alloy were conducted using both arc-melted as well as powder-metallurgy (PM) materials. The PM alloys were processed by grinding arc-melted buttons to -200 mesh powder using Si_3N_4 or steel balls and then consolidated using a two-stage technique. First, the powders were hot-pressed into cylinders in a graphite die at 1773 K under a stress of 31 MPa for 6 h in argon. Second, the hot-pressed cylinders were encapsulated in tantalum cans under vacuum and then further consolidated by hot isostatic pressing (HIP) at 1773 K under a pressure of 310 MPa for 2 h. The final compacts were nearly fully dense with little or no visible porosity (Fig. 5(a)). In contrast, the as-cast microstructure showed a large number of cracks despite the fact that the material was HIPed under similar conditions described above (Fig. 5(b)). Typical chemical compositions of the arc-melted and powder-metallurgy processed materials are shown in Table 4. The PM processing results in significant contamination of the alloy especially in its oxygen content, which increases to as much as about 1.0 at.%.

The alloy appeared to be resistant to most common chemical etchants. However, it could be etched electro-

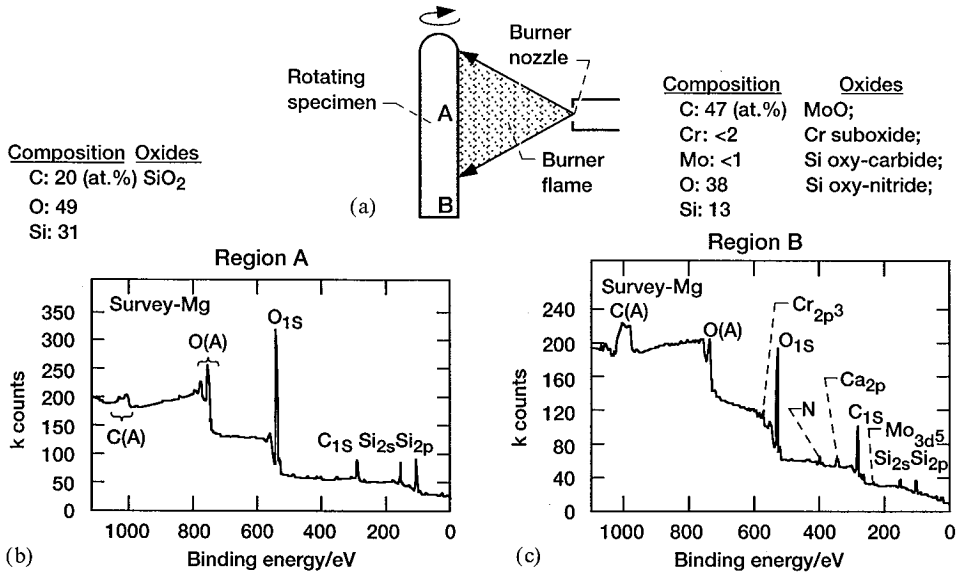

Fig. 4. (a) Schematic of the specimen configuration in the burner rig showing the areas which were analysed by X-ray photoelectron spectroscopy (XPS). (b) XPS data from the hot zone in region A showing an absence of Cr and Mo and the formation of SiO_2. (c) XPS data from region B away from the hot zone showing the presence of oxides of Cr, Mo and Si.

lytically in a 10% oxalic acid bath at room temperature under a polishing voltage of about 3 V to reveal the general microstructure. The $Cr_{40}Mo_{30}Si_{30}$ alloy consists primarily of two phases which were identified as M_3Si and M_5Si_3 by energy dispersive spectroscopy (EDS), where M = (Cr,Mo), although small amounts of a darker contrasting phase were often found to be associated with the latter (Fig. 5(c)). The major phases were confirmed by XRD and by transmission electron microscopy (TEM). Although preliminary analysis of this phase suggested that it is MSi_2 with an areal fraction in the microstructure of less than 1% [2,3], it should be noted that this identification may be in error. Instead, recent research suggests that the dark region also may be a M_5Si_3 phase but with a higher Cr content [24]. These results appear to indicate the possibility of spinodal decomposition occurring in this alloy system. Until further confirmation, this phase is identified as M_xSi_y in this paper (Fig. 5(c)). The formation of M_xSi_y may be influenced by chemical inhomogeneity and therefore it may not represent a true equilibrium phase corresponding to the nominal composition of the alloy. However, for practical purposes this material will be treated as a two-phase alloy in this paper since the area fraction of M_xSi_y phase is less than 1%. The areal fractions of M_3Si and M_5Si_3 were determined to be 48.2

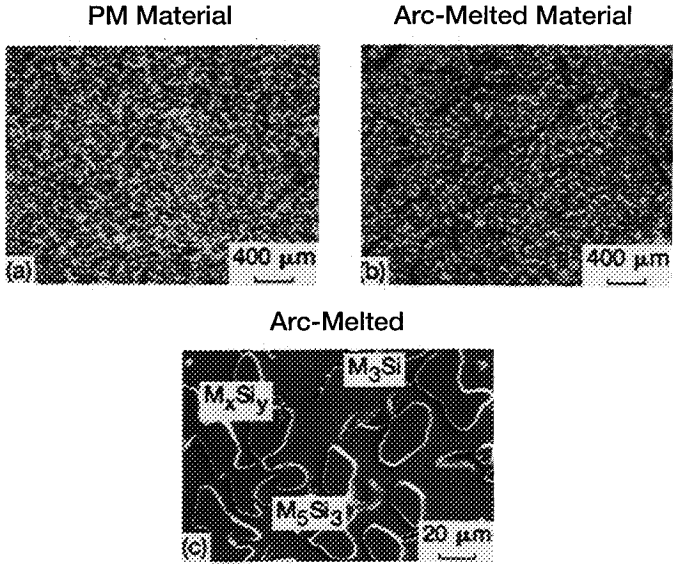

Fig. 5. Microstructures of (a) powder metallurgy-processed and (b) arc-melted and HIPed alloys. The PM material is nearly fully consolidated while the arc-melted microstructure contained a large number of cracks. (c) Back-scattered electron imaging of an arc-melted and HIPed specimen showing a M_3Si matrix containing M_5Si_3 and M_xSi_y phases.

Table 4
Average compositions of the arc-melted and powder-metallurgy alloys in at.%

Process	Major elements (at.%)				Interstitial elements (at.%)		
	Cr	Fe	Mo	Si	C	N	O
Arc-melted alloys	40.5	0.1	31.4	27.9	0.114 (225)	0.014 (70)	0.018 (45)
PM alloys	39.4	0.4	31.7	27.2	0.163 (315)	0.026 (120)	1.022 (2650)

Numbers in parenthesis represent p.p.m. values by weight. Cr, Mo and Si were determined by wet chemical analysis, while Fe was evaluated by the induction coupled plasma technique; C was analysed by the combustion extraction technique, while N and O were determined by the inert gas fusion method.

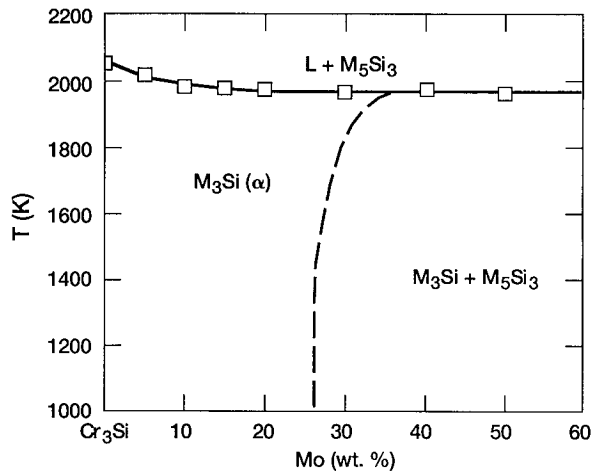

Fig. 6. Variation of the DTA peak with Mo substitution for Cr in Cr_3Si. The solidus line represents the melting point of the M_3Si phase. The broken curve demarcates the α and the two-phase M_3Si–M_5Si_3 phase fields.

and 49.2%, respectively. It should be noted that the grain boundaries were not visible in either of the major phases so that a grain size determination was not possible.

Differential thermal analysis (DTA) was used to determine the effect of Mo on the melting point of Cr_3Si using a Netzsch analyser. These measurements were conducted by heating small specimens (400–800 mg) in high purity alumina crucibles to 2073 K at a rate of 600 K h^{-1}. The choice of this maximum temperature range was determined in part by a need to prevent damage to the temperature sensors of the equipment and in part to ensure there was no reaction of the specimen with the crucible. The tests were conducted in a helium atmosphere flowing at a rate of 0.5–1.0 ml s^{-1}. The sample was then cooled from 2073 K to room temperature at the same rate. At least, three heat–cool cycles were employed to ensure reproducibility of results and minimize the possible influence of compositional segregation. In general, there was no evidence that the alloys reacted with the crucible below 2073 K. Since the effect of segregation on these results was a major concern, additional studies were conducted on the $Cr_{40}Mo_{30}Si_{30}$ alloy. In this case, measurements were conducted both on an arc-melted and on a heat-treated specimen, where the latter was soaked at 1673 K for 200 h. The DTA peak temperatures were nearly identical for both specimens. Additionally, batch to batch reproducibility was checked by obtaining DTA curves on specimens from different melts. These results were also sufficiently similar to ensure confidence in the data.

Fig. 6 shows a plot of the DTA peak temperature against the amount of Mo in wt.% substituted for Cr in Cr_3Si. The $Cr_{40}Mo_{30}Si_{30}$ alloy corresponds to the 50 wt.% Mo substitution. Only a single peak was observed in the DTA curves for all compositions in the temperature range 300–2073 K despite repeating the heat–cool cycles on the same specimen several times. Since the melting point of Cr_3Si is 2043 K [6], it is concluded that the DTA peaks correspond to the melting temperatures of the M_3Si phase and that the M_5Si_3 phase melts above 2073 K. The solidus temperature drops by 70 K with increasing Mo content from 2043 K for Cr_3Si to 1973 K until about 15 wt.% Mo. The solidus temperature is constant for higher Mo compositions. The broken curve in Fig. 6 represents the two-phase boundary which occurs at about 25 wt.% Mo. The position of this boundary, which is approximate, is based on preliminary optical and transmission electron microstructural (TEM) and X-ray diffraction (XRD) studies, but a precise determination is required from more detailed heat treatment experiments.

4. Property assessment

The oxidation and creep data were obtained on arc-melted specimens, while compression, creep, fracture toughness and physical property measurements were conducted on the PM materials. Mechanical testing was conduted on 3 × 3 × 7 mm specimens while the oxidation coupons were 10.0 mm in diameter and 2.5 mm thick. The specimens were electro-discharge machined (EDM) from the arc-melted and PM materials and polished to a surface finish of about 10 μm.

4.1. Physical properties

The melting point of the alloy was found to be about 1973 K, which is 70 K lower than that for Cr_3Si (Fig. 6). The specific gravity of the fully consolidated alloy was measured by the displacement technique to be 7.2 Mg m^{-3} while E at room temperature was determined to be 295 GPa by an impulse excitation vibrational technique. In comparison, $\rho \approx 8.7$ Mg m^{-3} and $E \approx 240$ GPa for commercial superalloys [16] while $\rho \approx 6.5$ Mg m^{-3} [5] and $E \approx 350$ GPa for Cr_3Si [11]. The room temperature thermal diffusivity, θ, measured by the pulse heating method was found to be about 4.8×10^6 m^2 s^{-1}. Noting that the thermal conductivity, β, is empirically related to θ through $\beta \approx 3 \times 10^6$ θ [25,26], the room temperature value of β is estimated to be about 14 W m^{-1} K^{-1}, which is twice that for a Ni–base superalloy but much lower than the reported values of about 78 and 50 W m^{-1} K^{-1} for NiAl and $MoSi_2$, respectively [16].

The CTE of the alloy was measured using an Orton dilatometer. These measurements were conducted on a 25 × 5 × 3 mm specimen between room temperature and 1773 K in an argon atmosphere, where the heating rate was controlled at 180 K h^{-1}. Measurements were made during three heat–cool cycles and the data were

found to be fairly reproducible. Fig. 7 compares the temperature dependence of the instantaneous coefficient of thermal expansion (CTE) for the present alloy with those for other materials [27]. The CTE for $Cr_{40}Mo_{30}Si_{30}$ increases from about 9×10^{-6} K^{-1} at room temperature to about 15×10^{-6} K^{-1} at about 1800 K (Fig. 7). As is evident from Fig. 7, the thermal expansion properties for $Cr_{40}Mo_{30}Si_{30}$ are intermediate between those of NiAl and $MoSi_2$. In addition, Fig. 7 suggests that long fiber composites using Al_2O_3 or Si_3N4 as reinforcements in a $Cr_{40}Mo_{30}Si_{30}$ matrix are likely to result in fiber–matrix debonding and matrix cracking during processing or thermal cycling due to the large CTE mismatch between the fibers and the matrix.

4.2. Oxidation properties

Thermogravimetric specific weight change measurements were conducted under both cyclic and isothermal oxidation conditions in the temperature range 1423–1573 K. In the cyclic tests, the oxidation coupons were cycled in static air between test and room temperatures, where the samples were maintained at temperature for 55 min followed by a 5 min cool down and the weight change was monitored continuously during the course of the test. The specimens were periodically removed from the furnace for an XRD determination of the composition of the oxide scale and for microstructural observations. Two types of isothermal test were conducted. First, the isothermal tests were conducted at 1473 and 1573 K in oxygen flowing at rates between about 0.3 and 1.7 ml s^{-1}, where the specimen weight change was recorded continuously for 100 h after which the oxide scale was analysed by XRD. Second, specimens were heated in air in muffle or tubular furnaces maintained at temperatures between 773 and 1673 K for various lengths of time. In some of these tests,

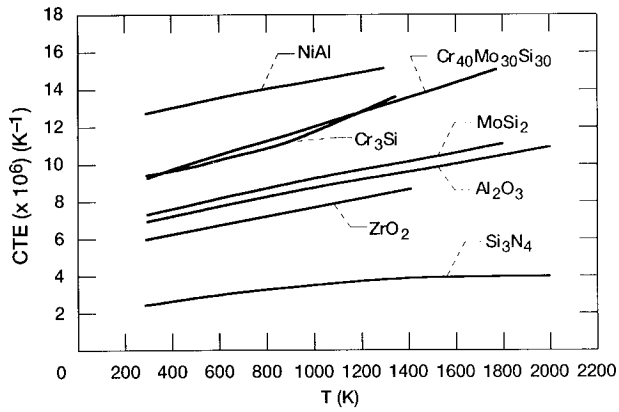

Fig. 7. Comparison of the temperature dependence of the instantaneous coefficient of expansion for $Cr_{40}Mo_{30}Si_{30}$ determined from thermal linear expansion data with those for Al_2O_3, Cr_3Si, $MoSi_2$, NiAl, Si_3N_4 and ZrO_2 [27].

Table 5
Comparison of the specific weight change for $Cr_{40}Mo_{30}Si_{30}$ after isothermal oxidation with those for several high melting point silicides [28]

Silicide	Oxidation temperature (K)	Oxidizing time (h)	$\Delta W/A$ (mg cm^{-1})
$MoSi_2$	1473	4	+0.3
	1773	4	+1.3
WSi_2	1473	4	−17
	1773	4	−23
$NbSi_2$	1473	6	+40
$TaSi_2$	1473	4	+60
$TiSi_2$	1473	4	+22
Mo_5Si_3	1773	4	−67
W_5Si_3	1773	4	−205
Ta_5Si_3	1773	1	+125
Ti_5Si_3	1773	2	+32
$Cr_{40}Mo_{30}Si_{30}$	1473	4	+0.3
	1473	100	−1.8
	1573	4	+0.6
	1573	100	−0.4

which were specifically designed to determine whether the alloy is susceptible to catastrophic oxidation or "pest" [9,10], a single specimen with pre-existing cracks was exposed for 200 h at each temperature between 773 and 1673 K. The weight change and the nature of the oxide scale were determined at the end of this 200 h exposure at temperature. "Pest" studies were also conducted on a specimen exposed at 773 K for 2000 h. The composition of the oxide scale was determined by XRD in all instances.

Table 5 compares the specific weight change undergone by the present alloy with those for other silicides under isothermal oxidation conditions [28]. It is evident from Table 5 that the alloy possesses excellent oxidation resistance compared to many other silicides. For example, the observed values of $\Delta W/A$ were -1.8 and -0.4 mg cm^{-2} after 100 h exposures at 1473 and 1573 K, respectively. In contrast, with the exception of $MoSi_2$, for which $\Delta W/A \approx +0.3$ mg cm^{-2}, the values of $\Delta W/A$ range between -17 and $+60$ mg cm^{-2} for the other silicides for exposures varying between 4 and 6 h at 1473 K. However, unlike $MoSi_2$, which catastrophically disintegrates or "pests" during oxidation at intermediate temperatures [9,10], $Cr_{40}Mo_{30}Si_{30}$ is stable during oxidation even if specimens with surface cracks are exposed for 2000 h at 773 K. For example, Fig. 8 demonstrates that a specimen with pre-existing cracks shows no signs of "pesting" after 200 h exposures at several temperatures between 773 and 1673 K. This result is not surprising since the alloy forms two protective oxide scales of Cr_2O_3 and SiO_2 (α-crystobalite) depending on temperature (Fig. 9). As shown in Fig. 9, the specific weight change is quite small ($\Delta W/$

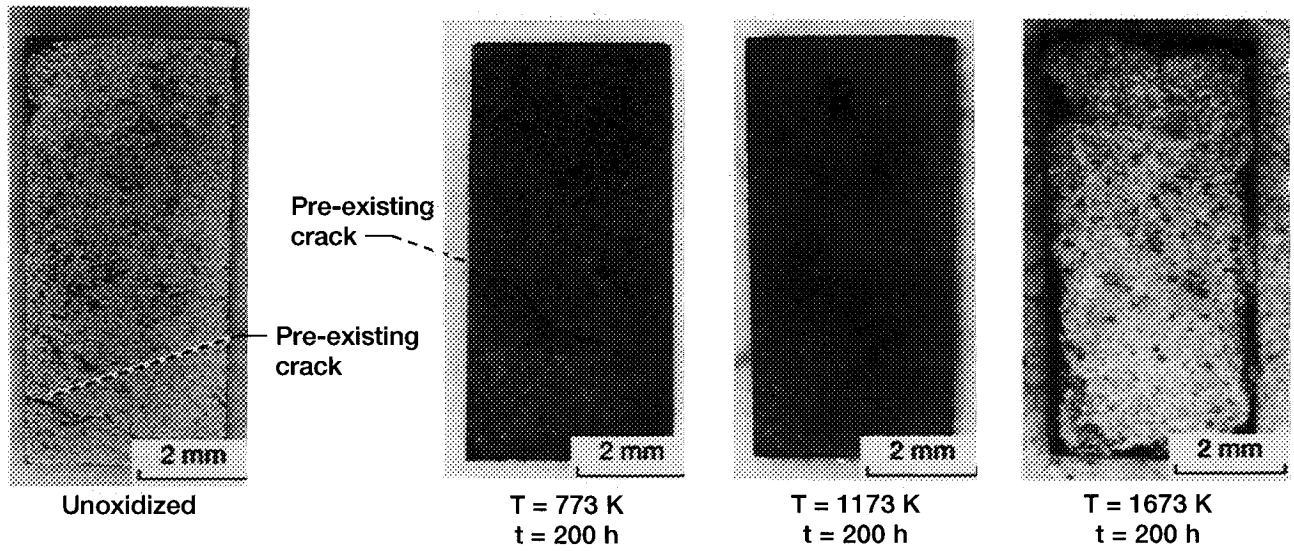

Fig. 8. Macrographs of a $Cr_{40}Mo_{30}Si_{30}$ specimen containing pre-existing cracks showing no evidence of "pest" or catastrophic oxidation. The specimen was exposed at several temperatures varying between 773 and 1673 K for 200 h at each temperature.

$A < 1$ mg cm^{-2}) below 1400 K but the specific weight loss increases above this temperature to about -14 mg cm^{-2} at 1673 K. In comparison, the calculated values of $\Delta W/A$ for $MoSi_2$ and NiAl are about 1 and 7 mg cm^{-2}, respectively, after 200 h at 1673 K based on typical values of k_p for SiO_2 and Al_2O_3 formation on these alloys [1].

Fig. 10 compares the specific weight change data at 1473 K for the cyclic and isothermal tests with crude estimates from the burner rig experiments. It is cautioned that the $\Delta W/A$ values for the burner rig data are imprecise since an accurate determination of the surface area of the oxidized regions of the specimen was not possible. Therefore, the inclusion of the burner rig data in Fig. 10 serves to provide only a qualitative comparison of the oxidation behavior of the alloy under these conditions with that under cyclic and isothermal oxidation conditions. The oxidation curves for the cyclic and isothermal tests are typical of Cr_2O_3 formers [29], where the specimens gain weight initially as the Cr oxidizes and then lose weight as the chromium oxides volatilize until a linear steady-state specific weight change is achieved. A comparison of the cyclic and isothermal data reveals a larger decrease in $\Delta W/A$ in the latter experiments presumably due to the effect of flowing O_2. In contrast to the cyclic and isothermal oxidation behavior, the alloy shows a relatively large decrease in $\Delta W/A$ during the early stages of the burner rig tests. This initial loss of matter is followed by a steady-state

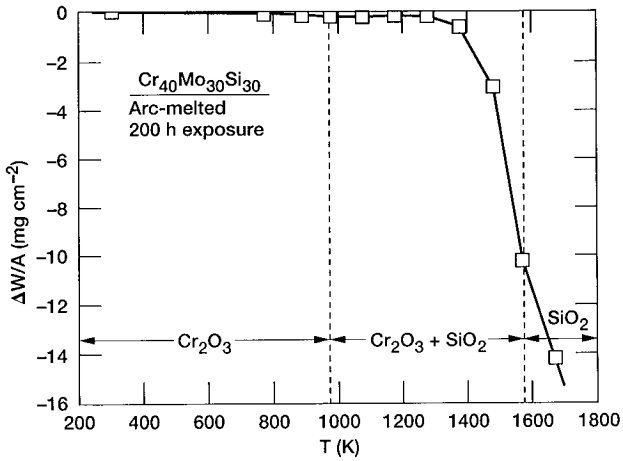

Fig. 9. Temperature dependence of the specific weight change in a $Cr_{40}Mo_{30}Si_{30}$ specimen exposed for 200 h at each temperature. The nature of the oxide scale as determined by XRD changes from Cr_2O_3 below 1000 K to SiO_2 above 1575 K.

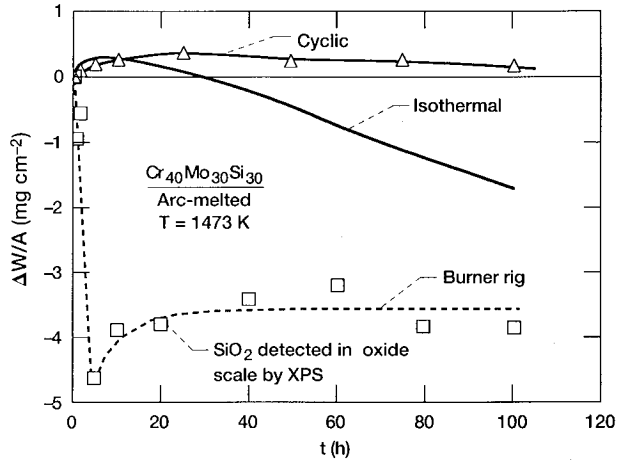

Fig. 10. Comparison of the time dependence of the specific weight change in $Cr_{40}Mo_{30}Si_{30}$ under cyclic, isothermal and burner rig oxidation conditions at 1473 K showing that the formation of a protective SiO_2 scale at the surface of the alloy in a burner rig test reduces weight loss. The larger weight loss in the isothermal tests in comparison to the cyclic experiments is probably due to the fact that the former were conducted in flowing oxygen while the latter measurements were carried out in static air.

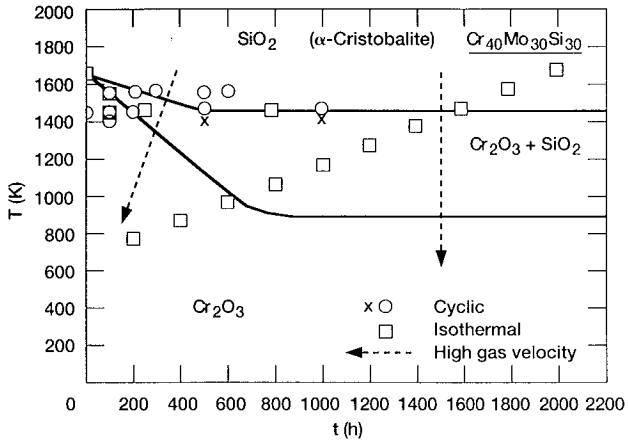

Fig. 11. Experimental oxidation map of absolute temperature vs. time for $Cr_{40}Mo_{30}Si_{30}$ showing the positions of Cr_2O_3 and SiO_2. The data were obtained from cyclic and isothermal tests. The broken arrows show the expected shift in the phase boundaries for oxidation under high velocity combustion gas.

region with little or no change in weight after the SiO_2 forms a protective layer at the surface (Fig. 10). Thus, the alloy is expected to perform extremely well under a high velocity combustion flame due to the rapid volatilization of Cr_2O_3 and the subsequent oxidation of the Si-rich external layer (Fig. 4(b)).

As noted earlier, the alloy forms two protective oxide scales consisting primarily of Cr_2O_3 at low temperatures and α-crystobalite (SiO_2) at high temperatures. The formation of SiO_2 appears to be dependent on the rate of volatilization of Cr_2O_3, which is dependent on temperature, time and gas velocity. This transition is illustrated in the experimental oxidation map showing the broad composition of the oxide scale for different combinations of oxidation temperatures and exposure times (Fig. 11). The isothermal data shown in Fig. 11 between 773 and 1673 K correspond to the specimen for which the specific weight change values are shown in Fig. 9. As described earlier, this specimen was exposed at each temperature for 200 h so that the exposure time shown in Fig. 11 for each datum point represents a cumulative time. It should be noted that a Cr_3O_4 spinel was sometimes observed in the scale along with Cr_2O_3 and SiO_2 at about 1500 K but for simplicity this information is excluded from Fig. 11. The boundaries are expected to shift to lower temperatures and shorter times under a high velocity combustion flame as depicted by the broken lines.

4.3. Mechanical properties

Constant engineering strain rate compression tests were conducted on $7 \times 3.5 \times 3.5$ mm PM specimens between room temperature and 1700 K, where these tests were conducted in air. Fig. 12 shows the compressive true stress, σ, vs. true strain, ε, curves for the PM material between 300 and 1700 K under an engineering strain rate, $\dot{e} \approx 1.0 \times 10^{-4}$ s^{-1}. The material is brittle below 1500 K, similar to Cr_3Si [12,13]. However, it deforms to plastic strains greater than 1% at and above this temperature. It is noteworthy that the material is quite strong even at 1500 K where its compressive strength is about 650 MPa but its strength decreases to about 50 MPa at 1700 K.

Constant load creep tests were conducted in air at 1500 K on $7 \times 3.5 \times 3.5$ mm arc-melted and PM specimens. The choice of this temperature was influenced in part by the fact that little measurable creep was observed in a specimen tested at a lower temperature of 1300 K under a stress of 150 MPa, and in part to allow a comparison with creep data on $MoSi_2$ alloys for which there are relatively few data below 1500 K. The effects of different processing techniques (i.e. arc-melted vs. PM) on the creep properties of the alloy are demonstrated in Fig. 13, where the secondary creep rate, $\dot{\varepsilon}$, has been plotted against the applied stress for data obtained at 1500 K. In the case of the arc-melted alloy, most of the data were obtained using a stress increase procedure although a few single specimen tests were also conducted to validate these results. The data on the PM alloy were obtained from single specimen tests. The effect of processing technique on the creep strength can be attributed in part to probable differences in the degree of refinement of the microstructure (e.g. grain size, precipitate size and inter-particle spacing) (Fig. 5(a) and (b)) and in part to variations in the impurity content (Table 4) between the arc-melted and PM materials. As mentioned earlier, the grain boundaries were not distinctly etched in this alloy so that the creep properties could not be directly correlated to variations in the grain size of the two differently-processed alloys.

Fig. 13 also compares the creep properties of the alloy with those of Cr_3Si [16], $MoSi_2$ [30], $Cr_{38}Mo_{39}Si_{23}$ [16], $MoSi_2$–20vol.%SiC_w whisker composites[3] [16,30] and $MoSi_2$–40vol.%SiC_p particulate composites [31], where data on these materials were obtained at 1473 K.

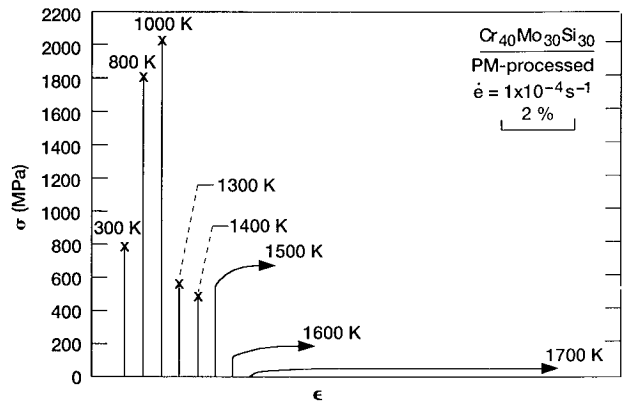

Fig. 12. Compression true stress vs. true strain for $Cr_{40}Mo_{30}Si_{30}$ between 300 and 1700 K.

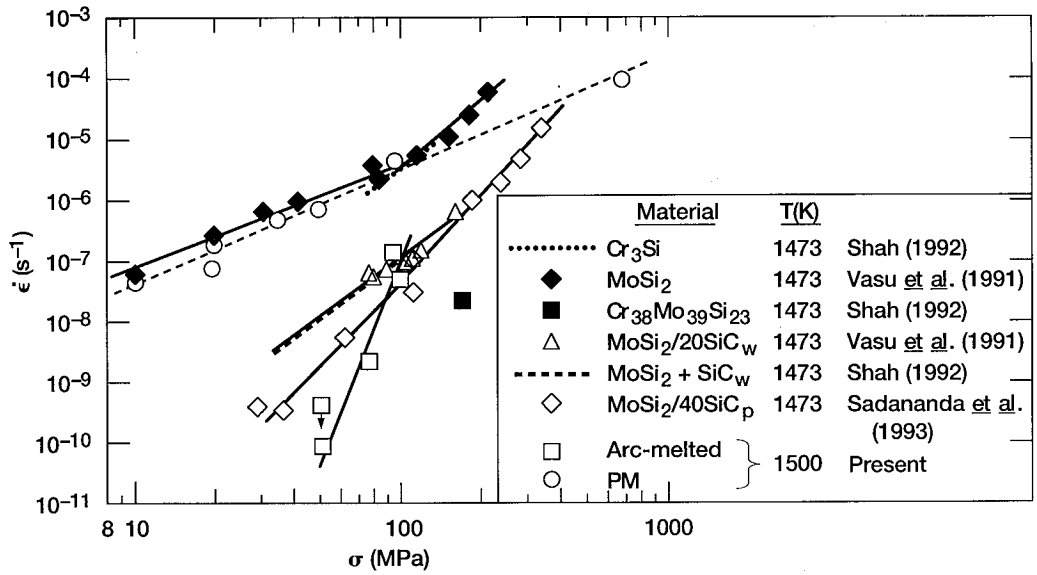

Fig. 13. Comparison of the stress dependence of the secondary creep rate for arc-melted and PM-processed $Cr_{40}Mo_{30}Si_{30}$ with those for Cr_3Si [16], $MoSi_2$ [30], $Cr_{38}Mo_{39}Si_{23}$ [16], $MoSi_2$–20vol.%SiC_w [16,30] and $MoSi_2$–40vol.%SiC_p [31].

It is clear that the creep strength of the PM material is similar to those of Cr_3Si [16] and $MoSi_2$ [30] below 100 MPa. In contrast, the arc-melted alloy is much stronger than $MoSi_2$–20vol.%SiC_w [16,30] below 100 MPa. Only $MoSi_2$–40vol.%SiC_p [31], deformed at a lower temperature of 1473 K, has similar creep strengths to the arc-melted $Cr_{40}Mo_{30}Si_{30}$ alloy. The single datum point for the $Cr_{38}Mo_{39}Si_{23}$ alloy [16] suggests that the latter alloy is stronger than the $MoSi_2$–SiC particulate and whisker-reinforced composites. More importantly, this observation provides an independent confirmation of the present results that Mo addition to Cr_3Si improves the creep properties of the latter. The role of Mo in improving the creep properties of Cr_3Si is unclear at the present time. It is important to note that this is a non-trivial problem since the role of other factors on creep strength, such as heat-to-heat compositional and microstructural variations, must be identified and understood before the effect of Mo can be elucidated. However, it is probable that Mo improves the creep strength of Cr_3Si by a combination of solid solution and precipitate hardening effects.

Room temperature fracture toughness measurements were conducted on bend specimens using the Single Edge Pre-cracked Beam (SEPB) technique [32]. These measurements were quite reproducible and the magnitude of K_q was determined to be between 2.0 and 3.0 MPa $m^{1/2}$. These values are much lower than those reported for the Cr–Cr_3Si eutectic alloys determined by a hardness indentation technique [17] but they are comparable with the values determined for $MoSi_2$ [33].

Although K_q for the present alloy is insufficient for practical applications, which are typically expected to require $K_q > 15$ MPa $m^{1/2}$, it is interesting to note that cracks were often observed to be deflected (Fig. 14(a)) and arrested (Fig. 14(b)) at the second phases in this alloy. This observation suggests that if the microstructure could be modified to a morphology where the second phase particles are elongated, then there may be some improvement in fracture toughness. However, significant improvements in toughness may be achieved only with the addition of possible toughening agents such as Y_2O_3-stabilized ZrO_2 or metal fibers coated with chemically inert coatings. In this connection, initial studies suggest that Y_2O_3-stabilized ZrO_2 is chemically inert in this alloy matrix.

The high hardness of the alloy, typically 1500–2000 HV, suggests that it is expected to have good wear resistance. Although there appear to be no published data on the wear resistance of Cr_3Si, it is interesting to note that Cr_3Si_2 possesses good wear resistance [34]. Thus, potential applications of the present alloy in the aerospace industry currently include erosion and oxidation resistant coatings on turbine airfoils as well as for use as combustor liners. Other possible spin-off applications for the alloy may exist if the wear resistance of the alloy is proven to be adequate. These include its use as a high temperature wear-resistant tool bit in the machine tool industry, and as a chemically inert extrusion die in the food, glass and polymer-processing industries, where despite the relatively low strength of the product, extrusion is conducted at high velocities in large tonnage of material. Ultimately, the choice of this alloy, as with any other material, will be determined by economic feasibility even if it possesses the desired combination of properties required for a particular application.

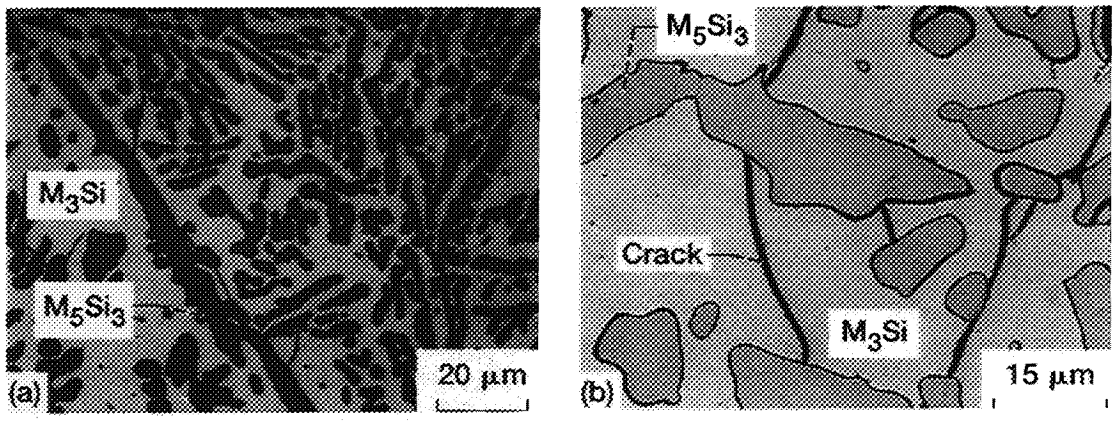

Fig. 14. Microstructure of an as-cast and HIPed $Cr_{40}Mo_{30}Si_{30}$ alloy showing (a) deflection and (b) arrest of the matrix cracks at the M_5Si_3 phase.

6. Summary and conclusions

An oxidation-resistant, two-phase M_3Si–M_5Si_3 alloy has been developed by alloying Cr_3Si with Mo. The alloy forms a protective Cr_2O_3 scale at low temperatures and α-crystobalite at high temperatures. The environmental resistance exhibited by the alloy suggests that it is well-suited for applications involving a high velocity combustion flame, such as in an aircraft engine environment. The physical properties of the alloy are equal to or better than those of commercial superalloys. The compressive creep strength of the arc-melted material is comparable to $MoSi_2$ with 40 vol.% SiC_p but the PM-processed alloy is only comparable in creep strength to unreinforced $MoSi_2$. The alloy also has a high compressive strength of 600 MPa at 1500 K. However, the fracture toughness of the alloy lies between 2.0 and 3.0 MPa $m^{1/2}$.

It is concluded from a preliminary assessment of the physical, mechanical and oxidation properties of $Cr_{40}Mo_{30}Si_{30}$ that the alloy appears suitable for use in non-structural applications in an aircraft engine, such as erosion and oxidation resistant coatings on turbine airfoils. However, unless the fracture toughness of the alloy can be improved substantially through the addition of toughening agents and by modifications of the microstructure, it cannot be used to fabricate critical load bearing components.

Acknowledgements

The author acknowledges the contributions of C. Barrett, R.M. Dickerson, R. Garlick, D. Jayne, I.E. Locci, J. Salem and J.D. Whittenberger.

References

[1] J.M. Nesbitt and C.E. Lowell, in I. Baker, R. Darolia, J.D. Whittenberger and M.H. Yoo (eds.), *High-Temperature Ordered Intermetallic Alloys V*, Vol. 288, Materials Research Society, Pittsburgh, PA, 1993, p. 107.
[2] S.V. Raj, *Proc. of the 3rd Int. Conf. on High-Temperature Intermetallics*, ASM International, Materials Park, OH, in press.
[3] S.V. Raj, *Mater. Sci. Eng., A, 192–193* (1995) 583.
[4] S. Bose, *Mater. Sci. Eng. A, 155* (1992) 217.
[5] Powder Diffraction File, American Society for Testing and Materials, Philadelphia, PA, card set 7-186, 1967, p. 211.
[6] A.B. Gokhale and G.J. Abbaschian, in T.B. Massalski, H. Okamoto, P.R. Subramanian and L. Kacprzak (eds.), *Binary Alloy Phase Diagrams*, Vol. 2, American Society for Metals, Metals Park, OH, 1987, p. 1333.
[7] E. Aitken, in J.H. Westbrook (ed.), *Intermetallic Compounds*, Robert E. Krieger, Huntington, NY, 1977, p. 491.
[8] D.A. Bertiss, R.R. Cerchiara, E.A. Gulbransen, F.S. Pettit and G.H. Meier, *Mater. Sci. Eng. A, 155* (1992) 165.
[9] E. Fitzer, in F. Benesovsky (ed.), *Second Plansee Seminar*, Springer, Vienna, 1956, p. 56.
[10] P.J. Meschter, *Metall. Trans. A, 23* (1992) 1763.
[11] R.L. Fleischer and R.J. Zabala, Mechanical properties of diverse binary high-temperature intermetallic compounds, *Report No. 89CRD201*, 1989, General Electric Research & Development Center, Schenectady, NY.
[12] C.S. Chang and D.P. Pope, in L.A. Johnson, D.P. Pope and J.O. Stiegler (eds.), *High Temperature Ordered Intermetallic Alloys IV*, Vol. 213, Materials Research Society, Pittsburgh, PA, 1991, p. 745.
[13] D.L. Anton and D.M. Shah, in O. Izumi (ed.), *Proc. Int. Symp. on Intermetallic Compounds — Structure and Mechanical Properties (JIMIS-6)*, The Japan Institute of Metals, Sendai, 1991, p. 379.
[14] D.M. Shah and D.L. Anton, *Mater. Sci. Eng. A, 153* (1992) 402.
[15] D.M. Shah, D. Berczik and D.L. Anton, *Mater. Sci. Eng. A, 155* (1992) 45.
[16] D.M. Shah, in S.D. Antolvich, R.W. Strusrud, R.A. MacKay, D.L. Anton, T. Khan, R.D. Kissinger and D.L. Klarstrom (eds.), *Superalloys 1992*, The Minerals, Metals and Materials Society, Warrendale, PA, 1992, p. 409.
[17] J.W. Newkirk and J.A. Sago, in D.L. Anton, P.L. Martin, D.B. Miracle and R. McMeeking (eds.), *Intermetallic Matrix Composites*, Vol. 194, Materials Research Society, Pittsburgh, PA, 1990, p. 183.
[18] B.P. Bewlay, J.A. Sutliff, K.M. Chang and M.R. Jackson, in V.A. Ravi and T.S. Srivatsan (eds.), *Processing and Fabrication*

of Advanced Materials for High Temperature Applications, The Minerals, Metals and Materials Society, Warrendale, PA, 1992, p. 213.

[19] K.M. Chang, B.P. Bewlay, J.A. Sutliff and M.R. Jackson, *JOM*, *44* (1992) 59.

[20] D.M. Shah and D.L. Anton, in R. Darolia, J.J. Lewandowski, C.T. Liu, P.L. Martin, D.B. Martin and M.V. Nathal (eds.), *First Int. Symp. on Structural Intermetallics (ISSI-1)*, The Minerals, Metals and Materials Society, Warrendale, PA, 1993, p. 755.

[21] R. Kieffer and F. Benesovsky, Symp. on Powder Metallurgy, The Iron and Steel Institute, London, *Special Report No. 58*, 1956, 292.

[22] D.W. McKee and R.L. Fleischer, in L.A. Johnson, D.P. Pope and J.O. Stiegler (eds.), *High Temperature Ordered Intermetallic Alloys IV*, Vol. 213, Materials Research Society, Pittsburgh, PA, 1991, p. 969.

[23] H.J. Grabke and M. Brumm, in T. Grobstein and J. Doychak (eds.), *Oxidation of High-Temperature Intermetallics*, The Minerals, Metals and Materials Society, Warrendale, PA, 1989, p. 245.

[24] R.M. Dickerson, S.V. Raj and I.E. Locci, in J. Horton, S. Hanada, I. Baker, R.D. Noebe and D. Schwartz (eds.), *High Temperature Ordered Intermetallic Alloys VI*, Materials Research Society, Pittsburgh, PA, 1995, Vol. 364, p. 949.

[25] M.F. Ashby, *Acta Metall.*, *37* (1989) 1273.

[26] M.F. Ashby, *Materials in Mechanical Design*, Pergamon, Oxford, 1992.

[27] Y.S. Touloukian, R.K. Kirby, R.E. Taylor and T.Y.R. Lee (eds.), *Thermophysical Properties of Matter: Thermal Expansion — Nonmetallic Solids*, Vol. 13, IFI/Plenum, New York, 1977.

[28] A.K. Vasudevan and J.J. Petrovic, *Mater. Sci. Eng. A*, *155* (1992) 1.

[29] C.E. Lowell, C.A. Barrett, R.W. Palmer, J.V. Auping and H.B. Probst, *Oxid. Metals*, *36* (1991) 81.

[30] A.K. Vasudevan, J.J. Petrovic and K. Sadananda, in N. Hansen et al. (ed.), *Proc. of the 12th Riso Ø Conference on Metal Matrix Composites*, 1991, p. 707.

[31] K. Sadananda, C.R. Feng, H.H. Jones and J.J. Petrovic, in R. Darolia, J.J. Lewandowski, C.T. Liu, P.L. Martin, D.B. Martin and M.V. Nathal (eds.), *First Int. Symp. on Structural Intermetallics (ISSI-1)*, The Minerals, Metals and Materials Society, Warrendale, PA, 1993, p. 809.

[32] S.R. Choi, A. Chulya, J.A. Salem, in R.C. Bradt et al. (eds.), *Fracture Mechanics of Ceramics*, Vol. 10, Plenum, New York, 1992, p. 73.

[33] J.J. Petrovic, A.K. Bhattacharya, R.E. Honnell, T.E. Mitchell, R.K. Wade and K.J. McClellan, *Mater. Sci. Eng. A*, *155* (1992) 259.

[34] T. Spalvins, *NASA TM X-73536*, Lewis Research Center, Cleveland, OH, 1977.

Instructions for Authors

SUBMISSION OF PAPERS

Manuscripts for the main part of the journal and for the Letters Section should be submitted as follows:

For authors in Europe

Editor-in-Chief
Professor Herbert Herman
Department of Materials Science and Engineering
State University of New York at Stony Brook
Long Island, NY 11794-2275, USA
Fax: +1 (516) 632 8052

or

Professor G. Kostorz
ETH Zurich
Institut fü Angewandte Physik
CH-8093 Zurich, Switzerland
Fax: +41 (1633) 1105

For authors in Japan

Professor Masahiro Koiwa
Department of Metal Science and Technology
Faculty of Engineering
Kyoto University
Yoshida-Honmachi, Sakyo-ku
Kyoto 606-01, Japan
Fax: +81 (75) 751 7844

For authors in North and South America and the rest of the world

Professor Herbert Herman
USA

Manuscripts

Three copies should be submitted to the Editor, in double-spaced typing on pages of A4 size and with wide margins (Letters should not exceed 2000 words and a maximum of 5 figures). All tables and illustrations should bear a title or legend.
An *abstract* should accompany reviews, original papers and Letters. It should present (preferably in 100–150 words; 50 words or less for Letters) a brief and factual account of the contents and conclusions of the paper, and an indication of the relevance of new material.
References should be indicated by numerals in square brackets, introduced consecutively and appropriately in the text.

References must be listed on separate sheet(s) at the end of the paper. Every reference appearing in the text should be quoted in the reference list, and *vice versa*. When reference is made to a publication written by more than two authors it is preferable to give only the first author's name in the text followed by "*et al.*" However, in the list of references the names and initials of all authors must be given.
Three sets of figures should be submitted. One set of line drawings should be in a form suitable for reproduction, drawn in Indian ink on drawing or tracing paper (letter height, 3–5 mm). Alternatively, such illustrations may be supplied as high contrast, black-and-white glossy prints. Duplicate original micrographs should be provided wherever possible to facilitate the refereeing process. Magnifications should be indicated by a ruled scale bar on the micrograph. Captions to illustrations should be typed in sequence on a separate page.
All abbreviated terms must be defined when first used (both in the abstract and in the text) and authors must express all quantities in SI units, with other units in parentheses if desired.
Authors in Japan please note that information about how to have the English of your paper checked, corrected and improved (before submission) is available from: Elsevier Science (Japan), 20-12 Yushima 3-chome, Bunkyo-ku, Tokyo 113; Tel: (03) 3833-3821; Fax: (03) 3836-3064.

Further information

All questions arising after the acceptance of manuscripts, especially those relating to proofs, should be directed to: Elsevier Editorial Services, Mayfield House, 256 Banbury Road, Oxford OX2 7DH, UK (tel. +44 1865 314900; fax. +44 1865 314990).

Submission of electronic text

The final text may be submitted on a 3.5 in or 5.25 in diskette (in addition to a hard copy with original figures). Double density (DD) or high density (HD) diskettes are acceptable, but must be formatted to their capacity before the files are copied on to them. The main text, list of references, tables and figure legends should be stored in separate text files with clearly identifiable file names. The format of these files depends on the word processor used. WordPerfect 5.1 is the most preferable but for other formats please refer to the Instructions to Authors booklet. It is *essential* that the name and version of the wordprocessing program, type of computer on which the text was prepared, and format of the text files are clearly indicated.
The final manuscript may contain last minute corrections which are not included in the electronic text but such corrections must be clearly marked on the hard copy.

0921-5093/95/$9.50

Printed in The Netherlands